Hyperspectral Images (HSI) Processing

Phevos A. Margonis - f3352317

December 5, 2023

Abstract

This paper is devoted to the processing of hyperspectral images, specifically focusing on spectral unmixing (SU) as a precursor to material label extraction. Our project aims to assess the performance of various regression algorithms in SU for extracting accurate labels of materials within the Pavia University dataset. Subsequently, these extracted labels serve as the basis for creating diverse classifiers, the efficiency of which is rigorously evaluated in material classification. The most effective classifier is then deployed operationally across different landscapes sharing common materials.

1 Introduction

In a real life scenario a small area, that is representative of the broader region under study, is examined by a human annotator. A sample of materials is collected in-order to form a baseline for comparison. Using those data, a Regression model is built that will take spectral signatures as input and as output it will try to break each signature down to its composite materials and their relative proportions. The nature of this problem dictates that the resulting proportions be positive and must sum to one for them to have a physical meaning.

This paper is centred around the examination of the pure pixels. Within those bounds a good Regression model is defined as one that is able to inflate the parameter of the actual material depicted, while deflating the parameters of the irrelevant materials. Subsequently, a series of different regression models will be examined to tackle the above challenge. The best one will be used to extract the inflated parameter and translate it into a label.

The result of the above experiment is a model that can adequately annotate materials over a larger region and it will be used to create a larger data set relating spectral signatures to labels. This new larger data set can be exploited to create a classifier that will input signatures and output labels with very high efficiency.

As will later be revealed, the task of accurately separating the spectral bands of materials is rather complicated, since some of them can have almost identical signatures. An efficient Classifier here is defined as one that will be able to distinguish the proper label of a material in any comparable situation.

2 Data exploration

In order to better understand the problem, we will first explore the available data. Firstly, we have a three-dimensional matrix named *HSI* that represents a specific scene of the Pavia University, taken from a satellite. The first two dimensions correspond to the spatial information. Each element of the spacial view is a pixel of the image and is represented by the radiance value of the mixture of materials depicted inside it. The third dimension corresponds to the spectral information of each pixel, divided in 103 bands.

Among the pixels containing a mixture of materials there are some that are composed of a single material, and will be hitherto referred as *pure pixels* (Table 1). The process of identifying those materials and their spectral signature is called Endmember Extraction. The result is the matrix *endmembers* which contains in its columns the spectral signature of 9 materials, with each row being a different band, and is depicted in Figure 2 where we have made an assumption for the names of the elements. Focusing in band 10 and relating it to the first image of Figure 1, using the reflectiveness of some surfaces, it is easier to make the connection between specific pixels and their materials.

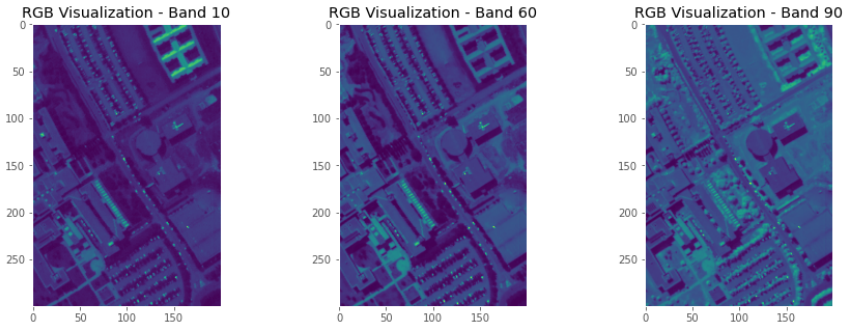

Figure 1: Three different bands of the HSI matrix

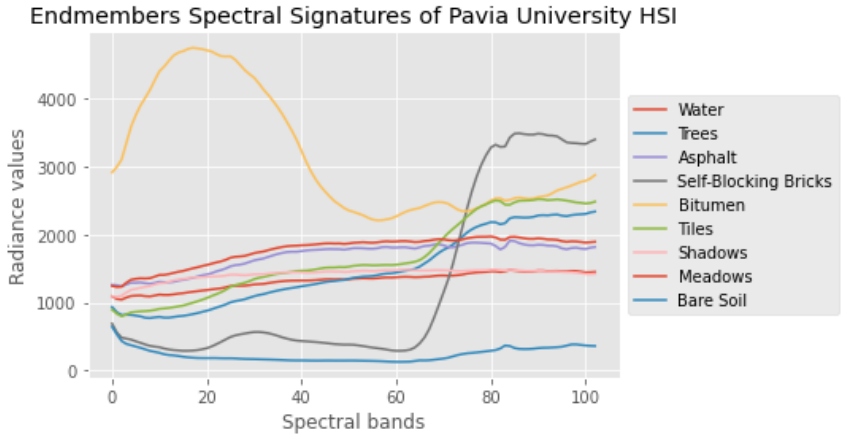

Figure 2: Spectral signature of each material

Finally, a matrix named *labels* is provided, which contains a number from 1 to 9 corresponding to the actual material of each pure pixel, and 0 for all mixed pixels, that acts as the ground truth and is used for comparison purposes.

Utilising the above connection and the labels, from now on for the sake of simplicity, we will focus our experimentation on a single pure pixel, and will refer to it as the *anchor pixel*. Pixel (30,150) of the HSI matrix depicts in Figure 1 a portion of a roof, which by convention is made out of *Bitumen* and is the 5^{th} element in the endmembers matrix. We can verify our assumption by plotting its spectral signature in Figure 3 and cross-examining its material in the matrix labesls.

Endmember	**Material**
1	Water
2	Trees
3	Asphalt
4	Self-Blocking Bricks
5	Bitumen
6	Tiles
7	Shadows
8	Meadows
9	Bare Soil

Table 1: Endmembers and corresponding materials. This is a naming convention and does not reflect the true correspondence of materials.

3 Spectral unmixing (SU)

In the following section, a series of different regression approaches will be utilised, in-order to untangle the relationship between the parameters of each pixel and the material depicted. The result of each regression model will be a three-dimensional matrix called *abundance map*. The

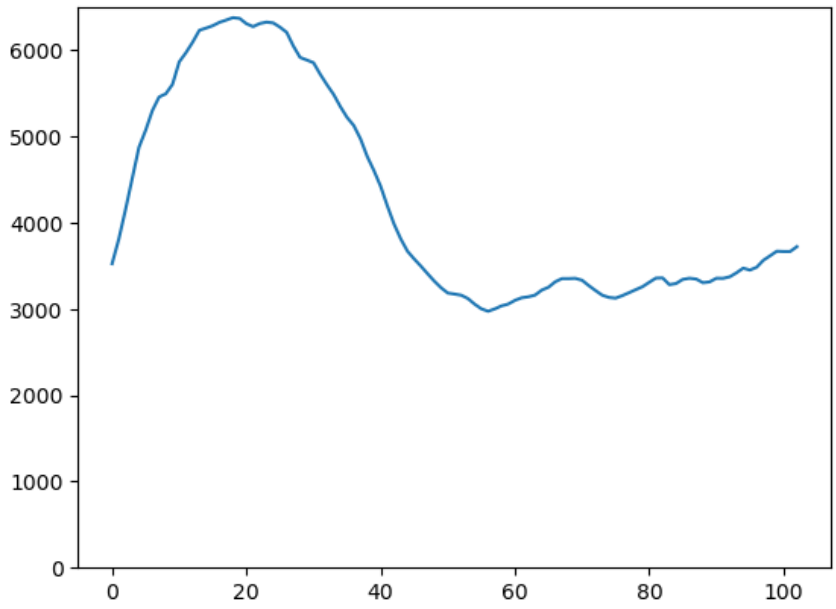

Figure 3: Spectral signature of anchor pixel (30,150)

first two dimensions correspond to the pixels, while the third corresponds to the parameters of the features that compose it.

To evaluate the different methods, a comprehensive set of measurements of the anchor pixel is used. Firstly, in Table 2 we present the parameters calculated from the model and in Table 3 we present the reconstruction error (which is calculated as $\frac{1}{N}||y_i - X\theta_i||^2$ of all the pure pixels). Consequently, we will compare the results obtained from the above five methods and try to demystify the results.

Finally, for each method the derived abundance map will be broken down to its respective materials. Then a figure will be drawn for each material. The best model will produce figures where the only highlighted parts, will be the pure pixels that correspond to that material.

3.1 Unconstrained Least Squares (LS)

The traditional least squares method has the lowest reconstruction error of all. This is due to the fact that no constraints are imposed on the cost function, and thus the model can fit more closely to the data set and its noise.

In the other hand, the resulted abundance map has no physical meaning and can not predict the material's label. Effectively, this method is disproportionately combining multiple materials in order to reach the target value of the dependent variable. From Figure 6 we can see that the produced images are very noisy and can not adequately separate the materials.

3.2 Sum-to-One (LS)

The reconstruction error in this method has increased slightly, and the prevailing parameter corresponds to the actual label. Although improved, this abundance map still is not representative of the physical meaning we are after. In Figure 7 we can see that the noise has decreased, but the materials are still not adequately separated.

3.3 Positive Parameters (LS)

As the values of the abundance map approach the desired formulation, we notice that the reconstruction error increases. This makes sense because we have introduced bias in our result in the form of the constraints, in-order to make the problem behave in the desired manner.

Now the irrelevant elements of the abundance map are all equal to 0 and the only non-zero element is the parameter corresponding to the actual label. Even still, the material proportions have no physical meaning. A significant change is presented in Figure 8 where the model has nullified the noise, making the material distinction easier. More importantly there is little to no miss-classification from map to map.

3.4 Fully Constrained (LS)

This approach demands that we constrain the parameters to be both positive and sum to one. This formulation represents the physical substance of the problem and is expected to outperform the others.

We have established the negative correlation of the parameter constraining and the reconstruction error, and such, here it peaks at its highest value. In contrast, the abundance map validates our hypothesis. The parameters of the irrelevant materials are zero, and the only material involved is equal to one.

Furthermore, the enhanced performance of this model becomes more evident when we conduct a comparative analysis of the 9^{th} Map of each model with that illustrated in Figure 9. This observation reveals a distinct improvement, as previously indistinguishable materials are now effectively highlighted.

3.5 Lasso Regularisation

By imposing the constraint of the first order norm of the parameters, we hope that the irrelevant ones will asymptotically shrink to zero. As we can see from the results, this simplistic approach does not have the desired effect, and in turn we get an intermediate solution between the first and second approach, independently of the value of the Lagrange coefficient. It is worth mentioning that by also applying the constraint of positive coefficients, the results are identical to that of the third approach.

The abundance map generated by this approach, as depicted in Figure 10, is notably intriguing. Despite existing evidence suggesting the potential for incorrect labels produced by this method, the discernibility of the depicted materials remains apparent. In numerous instances, these materials align accurately with their respective categories.

coef	LS	LS_SUM	LS_POS	CONVEX	Lasso
1	4.448	1.180	0.000	-0.000	3.422
2	-0.748	-0.474	0.000	-0.000	0.352
3	1.691	0.656	0.000	-0.000	-0.352
4	0.038	-0.003	0.000	-0.000	0.428
5	1.333	1.321	1.341	1.000	1.261
6	0.523	0.394	0.000	0.000	-1.714
7	-0.732	0.066	0.000	-0.000	-1.044
8	-3.941	-1.395	0.000	-0.000	0.067
9	-2.116	-0.745	0.000	-0.000	-2.308

Table 2: Parameter results for the anchor pixel. The model names represent (a) Unconstrained Least Squares LS, (b) Sum-to-One LS, (c) Positive Parameters LS, (d) Fully Constrained LS and (e) Lasso, respectively. Each coefficient(parameter) represents the proportion to which a material is involved in the mixture of the pixel. Refer to Table 1 for the material - coefficient correspondence.

Model	Rec. Error
LS	71.755
LS_SUM	82.447
LS_POS	139.258
CONVEX	263.279
Lasso	92.949

Table 3: Reconstruction error of all the pure pixels

4 Classification

In this section, four different classifiers are designed in order to discern the labels of pure pixels. The efficiency of each classifier is calculated with the score *accuracy*, which is calculated as

$$\frac{Number\,of\,correct\,clssifications}{Total\,number\,of\,observations}$$

A 10-fold cross-validation is applied in the data-set and the results are gathered in Table 4.

Model	**Mean**(%)	**Std**
Naive Bayes	64.5	0.057
MED	55.2	0.060
KNN	84.8	0.054
Bayesian	99.1	0.006

Table 4: Accuracy score of the 10-Fold cross-validation

Going back to Figure 2 it is worth noting the spectral signatures of the following sets:

- Trees - Tiles
- Meadows - Asphalt
- Shadows - Water

What we realize is that these pairs have almost identical signatures that are overlapping or are slightly shifted. This is particularly challenging for more naive approaches, since those minute differences could be confused as noise.

Following the 10-Fold cross-validation, each model is being trained in the entirety of the training data set and then is assessed using the test data set. A confusion matrix is then calculated for each model. The diagonal elements of each matrix in Figure 5 represent the numbers of correct classifications, while all the rest represent the wrong classifications.

4.1 Minimum Euclidean Distance

This method is a special case of the Bayes classifier that makes the assumption that the classes (a) are equiprobable, and (b) are modelled by normal distributions of equal diagonal covariance matrices of the form $\sigma^2 I$. Effectively, the class is calculated as $argmin(||x - \mu_q||)$ and thus no other information is accounted past the distance of the point under study from the centre of each class. Since the accuracy score is so low 55.78%, we can infer that the data do not meet the aforementioned requirements.

By examining the corresponding confusion matrix, we can see significantly inflated numbers in the off-diagonal elements, especially in the sets with similar signal. Consequently, we validate the hypothesis that those pairs will pose a challenge for our classifiers and thus the need arises for further experimentation.

4.2 Naive Bayes

In utilising the Gaussian Naive Bayes classifier we have made the assumption that the classes follow a normal distribution and all the features are statistically independent, from each other. The accuracy score of 66% in this case is slightly better than the minimum euclidean distance, but the classifier still struggles in the same areas.

4.3 K-Nearest-Neighbour

The algorithm of K-Nearest-Neighbour is a non-parametric classifier, and thus we do not need to make any assumptions about the distributions of the features. The only hyper-parameter we need to fine-tune in this case, is the number of neighbouring points the algorithm should take into consideration. To achieve this, we make use of the *Elbow* method, where we run multiple instances with different k values. By plotting the resulting accuracy in Figure 4, we can see that the most prominent values lie around k=5.

The kNN algorithm achieves a score of 88.6% in the test-set, which is surprising for its simplistic approach. In order to verify that there was no over-fitting on the hyper-parameter leaked in the test-set, the *Operational* set is employed, which scores at 91% accuracy.

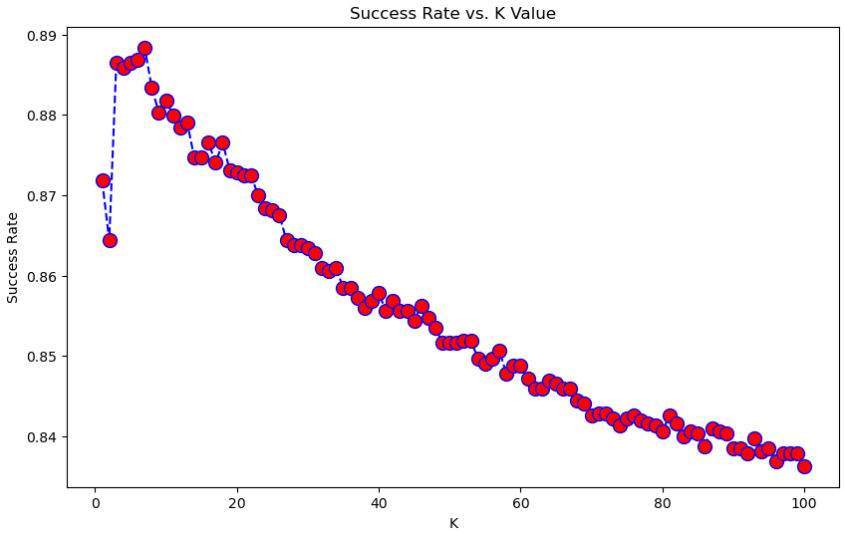

Figure 4: Elbow method for kNN

4.4 Bayes Classifier

In utilising the Gaussian Bayes classifier we have made the assumption that the classes follow a normal distribution of different covariance matrices. This method scores 99.1% accuracy in the training set, 88.4% in the test set, and 76.8% in the operational set. It is clear that taking into account the full covariance matrices of the classes, leads to over-fitting.

In both kNN and Bayes classifier the only significantly inflated elements, in the off-diagonal positions of the confusion matrices, are limited to the aforementioned signal-pairs, and in areas their signals overlap.

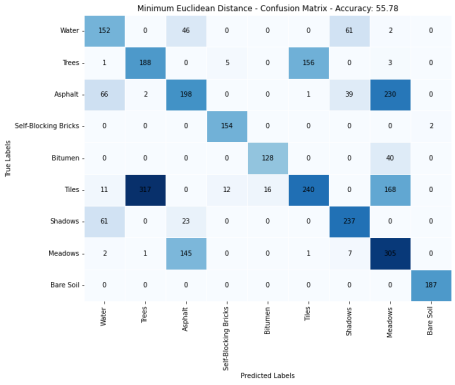

(a) Minimum Euclidean Distance

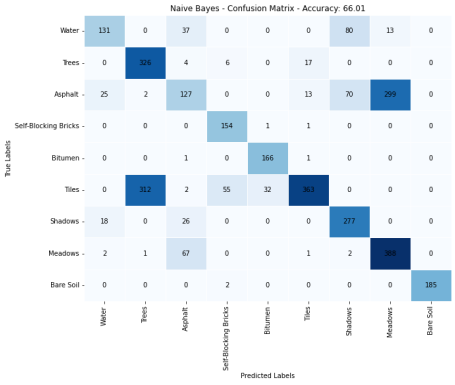

(b) Naive Bayes

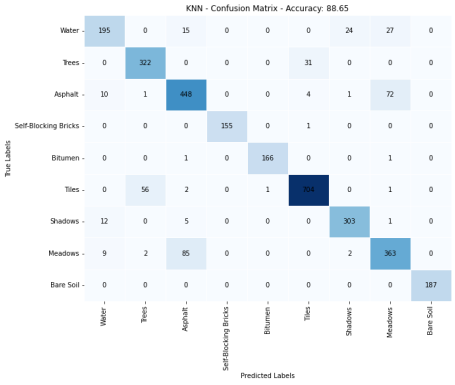

(c) KNN

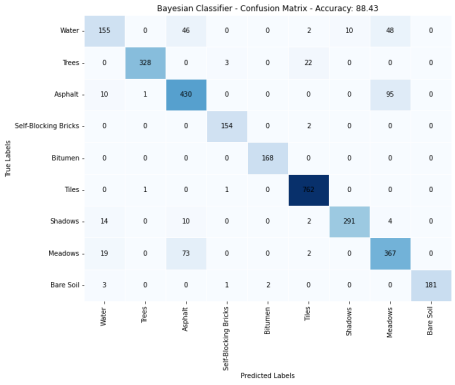

(d) Bayes

Figure 5: Confusion matrices of classifiers

5 Conclusion

In conclusion, we have underscored the necessity of imposing constraints on parameters—specifically, non-negativity and a collective sum to one—to develop a robust regression model. Subsequently, employing the *argmax* in each element of the abundance map enables the extraction of labels for spectral bands. This model can be applied to a more expansive area to procure a more extensive dataset of spectral signals and their corresponding labels. This enlarged dataset, in turn, serves as the foundation for designing a classification model adept at swiftly translating spectral signals into labels. Finally, we have substantiated that, given the approximation of classes by normal distributions, the most resilient classification model involves the utilisation of the non-parametric kNN algorithm.

A Appendix: Additional Material

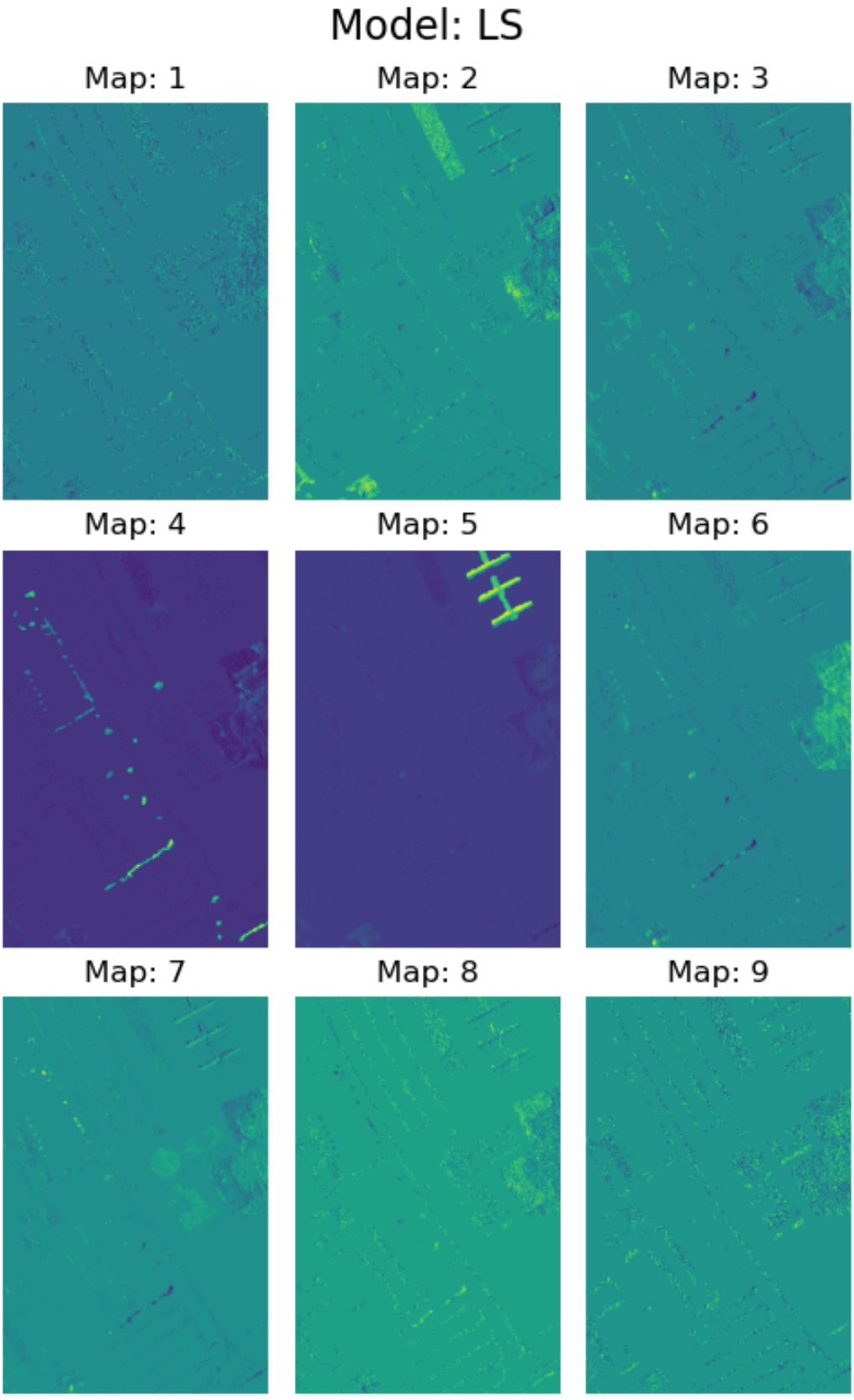

Figure 6: Abundance maps for the Unconstrained Least squares

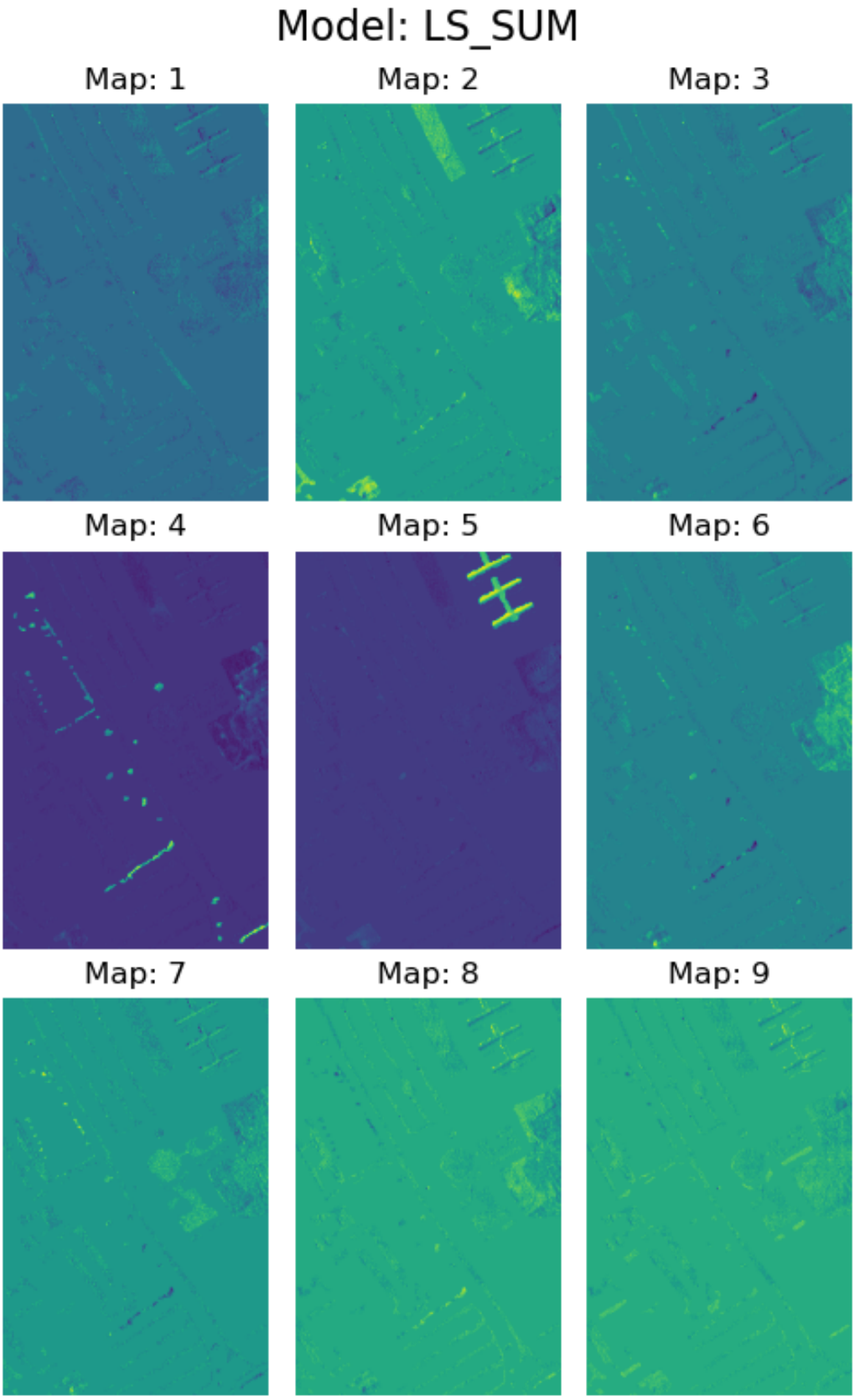

Figure 7: Abundance maps for the Sum-to-One Constrained Least squares

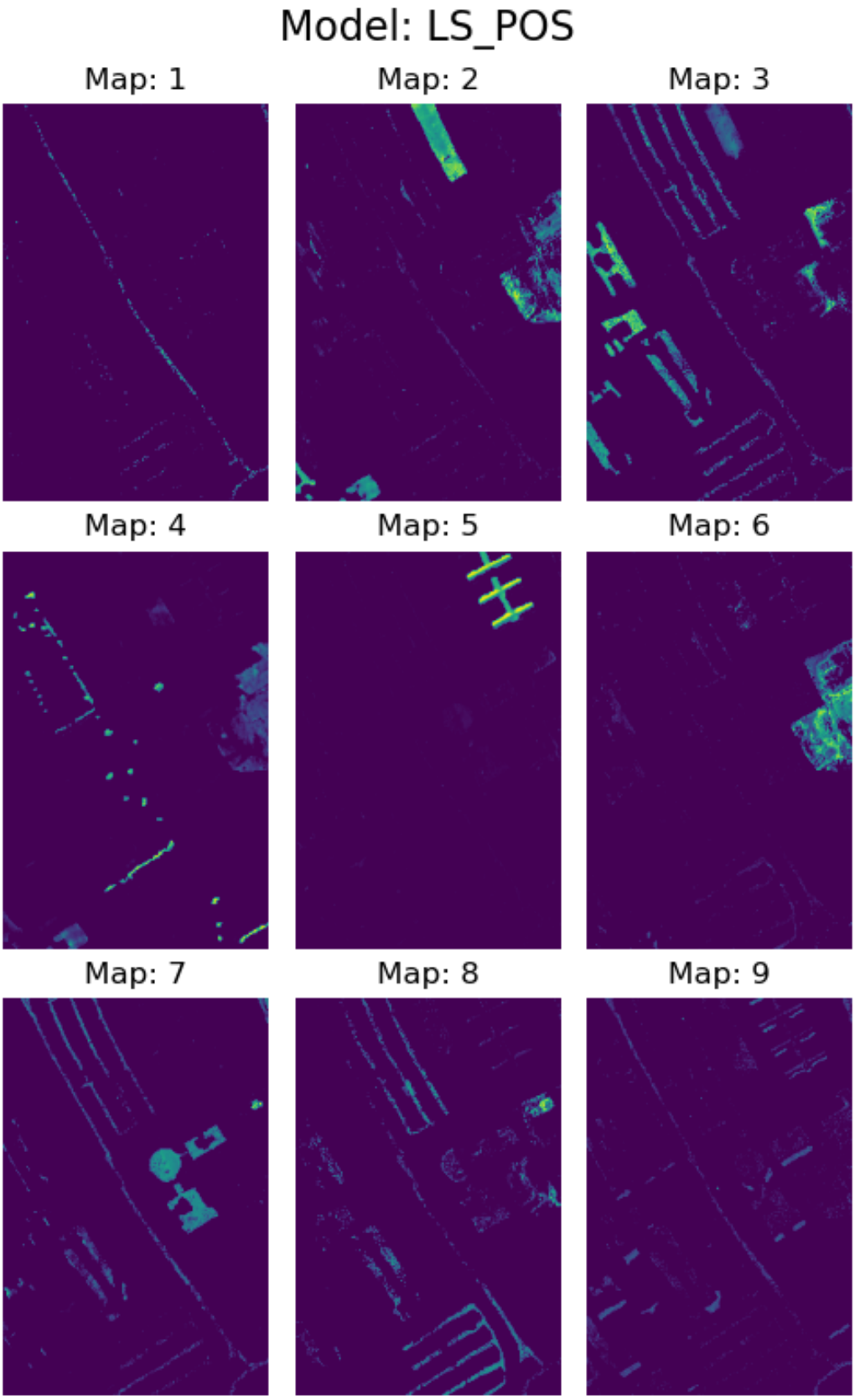

Figure 8: Abundance maps for the Positive-Coefficients Constrained Least squares

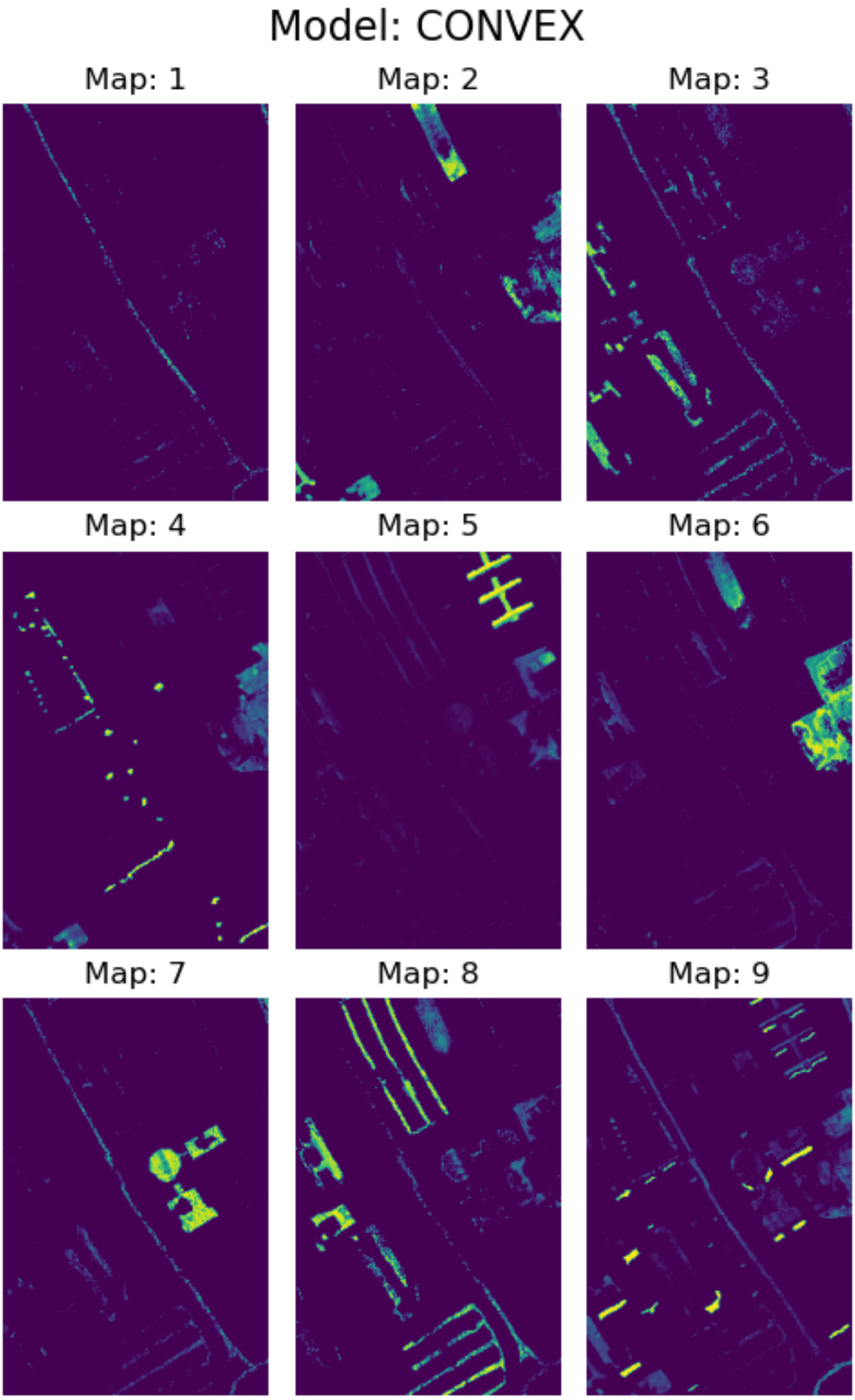

Figure 9: Abundance maps for the Fully Constrained Least squares

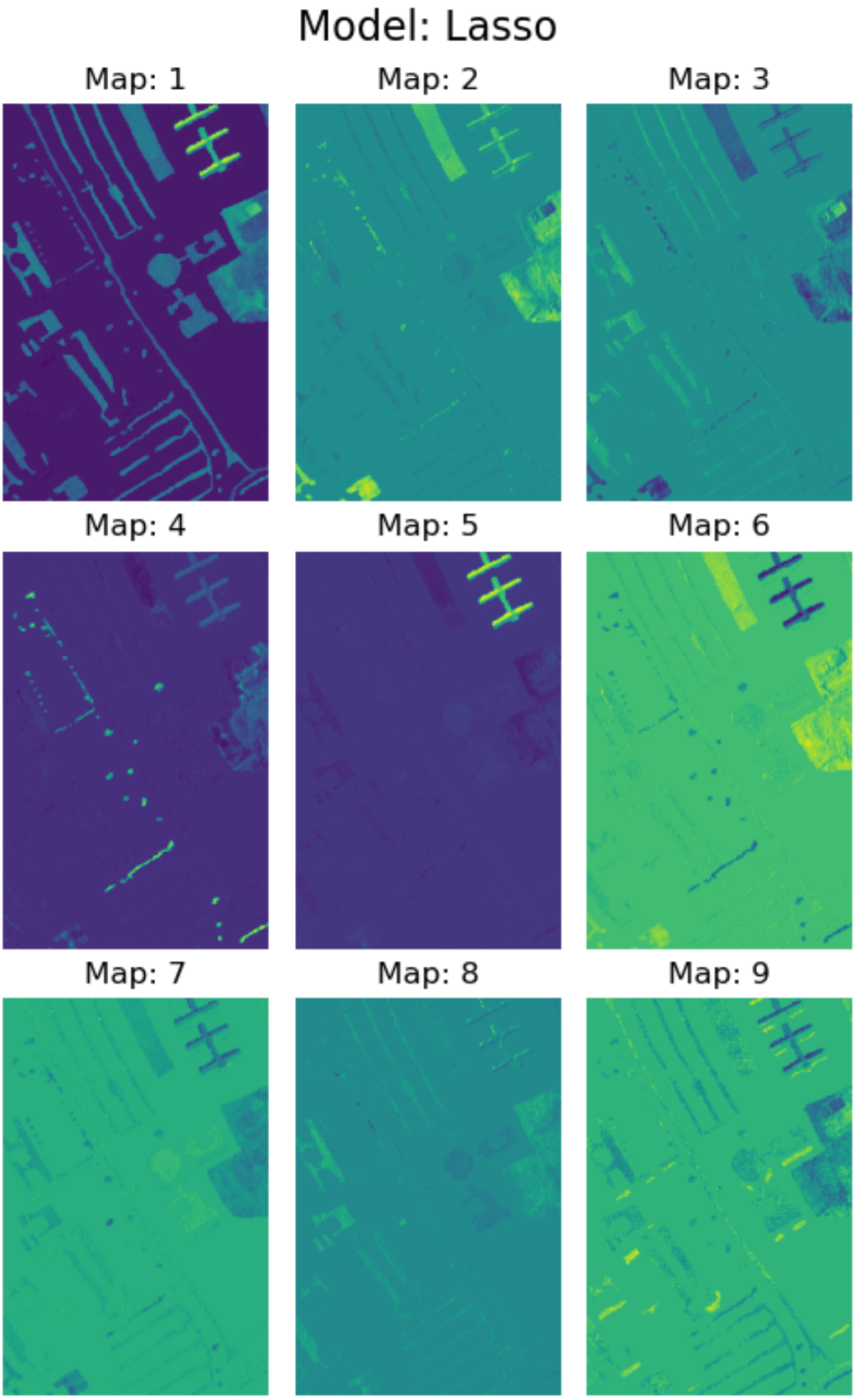

Figure 10: Abundance maps for the Lasso Regularisation